

Quantum interference of a single spin excitation with a macroscopic atomic ensemble

S. L. Christensen, J.-B. Béguin, E. Bookjans, H. L. Sørensen, J. H. Müller, J. Appel,* and E. S. Polzik*
QUANTOP, Niels Bohr Institute, University of Copenhagen, Blegdamsvej 17, 2100 Copenhagen, Denmark

We report on the observation of quantum interference of a collective single spin excitation with a spin ensemble of $N_a \approx 10^5$ atoms. Detection of a single photon scattered from the atoms creates the single spin excitation, a Fock state embedded in the collective spin of the ensemble. The state of the atomic ensemble is then detected by a quantum nondemolition measurement of the collective spin. A macroscopic difference of the order of $\sqrt{N_a}$ in the marginal distribution of the collective spin state arises from the interference between the single excited spin and N_a atoms. These hybrid discrete-continuous manipulation and measurement procedures of collective spin states in an atomic ensemble pave the road towards generation of even more exotic ensemble states for quantum information processing, precision measurements, and communication.

PACS numbers: 42.50.Dv, 42.50.Lc, 03.67.Bg

I. INTRODUCTION

The development of interfaces between quantum systems plays a large role in present-day quantum information research. One of the most used interfaces is based on the interaction between light and atomic ensembles [1, 2]. Until now, predominantly, two different approaches based on either discrete or continuous variables have been used. The discrete method is based on collective single excitations, photon counting, and mapping of the atomic state into a photonic state which is then characterized [2–6]. The continuous-variable schemes use atomic homodyne measurements which allow for deterministic protocols, such as quantum teleportation [1, 7], spin squeezing and atomic tomography [8–10], quantum-assisted metrology [11–13], and quantum memories [1, 14]. A general feature of the continuous-variable approach is its high-efficiency state characterization and mode selectivity. Hybrid discrete-continuous quantum state generation has been demonstrated in pure photonic systems [15–19]. Here, we report on a hybrid discrete-continuous protocol combining a collective atomic excitation heralded by a single-photon count with a continuous measurement of the atomic state *directly* in the ensemble. In combination with quantum nondemolition (QND) measurement-induced squeezing [8], the discrete manipulation of the excitation number allows for creation of Schrödinger’s cat states [15] within a quantum memory which are a valued resource for quantum repeater protocols [20]. States created by this method can improve measurements beyond the standard quantum limit [21]. The experiment presented here unifies two main approaches to atom-light quantum interfaces: first, a single excitation is generated via a Raman-type process (where a direct retrieval would result in a single photon in the output mode) [5]; then, a Faraday-type (QND) memory readout [1] of the resulting interference is performed.

II. THEORY

Our experiment is conducted on an atomic ensemble of pseudo-spin-1/2 atoms following the proposal in [22]. It can be described in four simple steps. (i) All spins are oriented in one direction, and the prepared ensemble state is $|\Psi_0\rangle = |\uparrow\uparrow \dots \uparrow\uparrow\rangle$. (ii) A single spin is probabilistically flipped into the opposite state, without resolving which atom was affected such that the excitation is distributed over the ensemble. The system state becomes

$$|\Psi_1\rangle \equiv \frac{1}{\sqrt{N_a}} \sum_{l=1}^{N_a} |\uparrow\uparrow \dots \uparrow \underbrace{\downarrow}_{l\text{th atom}} \dots \uparrow\uparrow\rangle. \quad (1)$$

(iii) A $\pi/2$ pulse acting homogeneously on all atoms transfers each atom into an equal superposition: $|\uparrow\rangle \rightarrow |+\rangle$ and $|\downarrow\rangle \rightarrow |-\rangle$ with $|\pm\rangle \equiv \frac{|\uparrow\rangle \pm |\downarrow\rangle}{\sqrt{2}}$. Depending on the presence or absence of the spin flip, this leaves the system in one of the two following states:

$$|\Psi'_0\rangle = |++ \dots ++\rangle, \quad (2)$$

$$|\Psi'_1\rangle = \frac{1}{\sqrt{N_a}} \sum_{l=1}^{N_a} |++ \dots + \underbrace{-}_{l\text{th atom}} \dots ++\rangle. \quad (3)$$

(iv) Atomic state analysis is performed by measuring the population difference of atoms in the two spin states $\Delta N = N_+ - N_-$.

An interesting and somewhat counterintuitive observation is that the probability distribution of the measurement outcome is fundamentally altered whenever a single spin-flip has taken place. The magnitude of the difference between the spin-flip and no-spin-flip distributions is comparable to the atomic quantum projection noise ($\sim \sqrt{N_a}$) and is thus much bigger than an incoherent single-atom effect. This enhancement is explained by quantum interference between the single excited spin and the unaffected atoms.

The single-excitation state $|\Psi'_1\rangle$ has several interesting features: in the limit of a large ensemble, $N_a \gg 1$, the states $|\Psi'_0\rangle$ and $|\Psi'_1\rangle$ correspond to the atomic equivalent

* Corresponding Authors: polzik@nbi.dk; jappel@nbi.dk

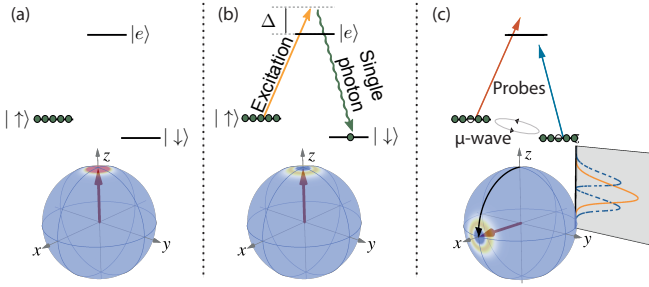


FIG. 1. (Color online) The simplified atomic level structure and the collective Bloch sphere at different stages of the experiment. (a) All atoms are prepared in the $|\uparrow\rangle$ state via optical pumping. (b) Detection of a scattered anti-Stokes photon following a weak excitation of the ensemble signals that a single atom has been transferred to the $|\downarrow\rangle$ state. (c) A microwave $\pi/2$ pulse causes the single excited atom in $|\downarrow\rangle$ to interfere with the remaining atoms in $|\uparrow\rangle$ by rotating all spins into the equatorial plane. This creates the collective state $|\Psi'_1\rangle$, which is characterized by a continuous-variable measurement. The inset shows the probability density of \hat{J}_z for $|\Psi_0\rangle$ [solid orange] and $|\Psi'_1\rangle$ [dashed blue].

of the vacuum and single-excitation states of a bosonic mode (Holstein-Primakoff approximation [23]). Unlike a single-photon state which is superposed with a strong local oscillator on a beam splitter to reveal its Wigner function [24], in the present case the atomic ensemble plays the role of the local oscillator and is inseparable from the single spin carrying the excitation. The state $|\Psi'_1\rangle$ is non-Gaussian with a negative Wigner function stored within a quantum memory. As such it is potentially valuable for quantum information applications [5, 25, 26]. This negativity of the Wigner function leads to a non-Gaussian marginal distribution with an increased variance compared to $|\Psi_0\rangle$ [see inset in Fig. 1c [22]]. It is exactly this increase that we will use to distinguish between the two states of interest. In our experiment various technical imperfections (detector dark counts and so on.) limit the purity of the $|\Psi'_1\rangle$ -state preparation. As shown in detail later, this reduces the expected increase in the variance of the population difference. Due to the signal enhancement by interference, even for a low-purity state we are able to discriminate the created state against $|\Psi'_0\rangle$.

We employ an ensemble of approximately 10^5 cesium atoms; the pseudospin system is formed by two stable levels in the ground-state hyperfine manifold, the clock states $|\uparrow\rangle \equiv |F=4, m_F=0\rangle$ and $|\downarrow\rangle \equiv |F=3, m_F=0\rangle$. Each atom l is described by pseudospin operators $2\hat{j}_z^{(l)} = |\uparrow\rangle\langle\uparrow|^{(l)} - |\downarrow\rangle\langle\downarrow|^{(l)}$, $2\hat{j}_x^{(l)} = |+\rangle\langle+|^{(l)} - |-\rangle\langle-|^{(l)}$, and $\hat{j}_y^{(l)} = i[\hat{j}_x^{(l)}, \hat{j}_z^{(l)}]$. Introducing the collective operators $\hat{J}_i = \sum_{l=1}^{N_a} \hat{j}_i^{(l)}$, the ensemble state can be visualized on the Bloch sphere [see Fig. 1 [27]]. For the characterization of the interference effect, the observable of interest is $\hat{J}_z = \Delta N/2$.

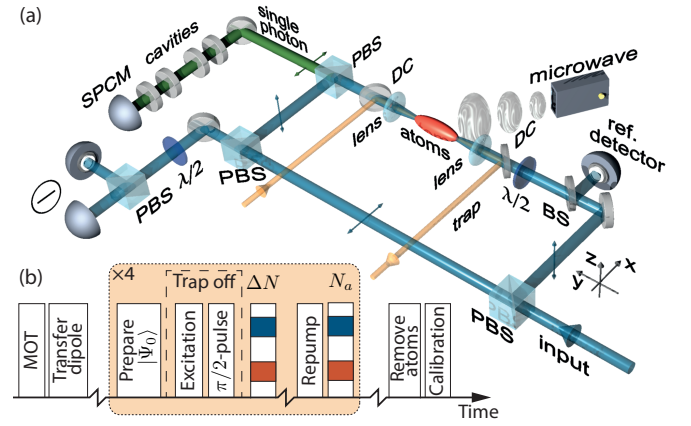


FIG. 2. (Color online) (a) Experimental setup. The dipole-trapped atomic ensemble is overlapped with one arm of a MZI, using dichroic (DC) mirrors. The input mode of the MZI is used for the weak Raman excitation and for the dual-color QND measurement of atoms. A single-photon counter module (SPCM) detects the heralding photon. To select a photon in the desired decay channel, polarization (via PBS) and frequency (via Fabry-Pérot cavities) filters are implemented. The atomic state is characterized by a dispersive QND measurement using balanced homodyne detection. A beam splitter (BS) is used to calibrate the probe power. (b) Pulse sequence.

III. EXPERIMENT

To create the state $|\Psi_0\rangle$, we first load atoms in a magneto-optical trap (MOT), transfer them into a dipole trap (formed by a $P \approx 4.7$ W, 1064 nm-laser beam), and optically pump them into the $|\downarrow\rangle$ state using the D_2 line [12]. With a microwave π pulse and a subsequent resonant $F = 3 \rightarrow F' = 4$ optical purifying pulse we bring the atoms into the $|\uparrow\rangle$ state and remove any remaining coherences between $|\uparrow\rangle$ and $|\downarrow\rangle$ [see Fig. 1a]. To minimize the inhomogeneous broadening of the optical transitions, we briefly turn off the dipole trap and subject the ensemble to a $2.5 \mu\text{s}$ off-resonant excitation pulse, detuned by $\Delta = 5.4$ MHz with respect to the $|\uparrow\rangle \leftrightarrow |e\rangle = |F' = 4, m_{F'} = 1\rangle$ transition, focused to a waist of $30 \mu\text{m}$ and comprising $n_{\text{exct}} = 8.9 \times 10^5$ photons. By independently measuring the reduction of the microwave π pulse contrast due to this excitation pulse, we infer that $1 - \eta_{\text{scatter}} = 23\%$ of the atoms scatter a photon from this excitation beam (see Appendix C: Scattering); with a probability $p_{\text{forward}} = 1.43\%$ the atoms forward scatter a photon with an energy corresponding to a decay to the $|\downarrow\rangle$ state exactly into the detection spatial mode. The detection of a *single* $|\uparrow\rangle \rightarrow F' = 4 \rightarrow |\downarrow\rangle$ anti-Stokes photon signals that a single atom has been transferred to the $|\downarrow\rangle$ state and thus heralds the preparation of the $|\Psi_1\rangle$ state [see Fig. 1b [5]]. Using a microwave $\pi/2$ pulse, we cause the single excited atom to interfere with the remaining $|\uparrow\rangle$ -state atoms [see Fig. 1c] and reestablish the dipole trap.

The atoms are held in one arm of a Mach-Zehnder

interferometer (MZI) [see Fig. 2a], which allows us to measure $\hat{J}_z \propto \Delta N$ by dual-color QND tomography [12] with a precision much better than the projection noise using $n_{\text{probe}} = 1.51 \times 10^8$ photons in total [see Fig. 1c]. We then repump all atoms into $F = 4$ and determine N_a , by again measuring the atomic induced phase shift [8]. Depending on the detection of the heralding anti-Stokes photon, the measurement outcomes are associated with \hat{J}_z statistics of either the $|\Psi'_0\rangle$ or $|\Psi'_1\rangle$ states. To optimize the measurement time we reuse the same MOT cloud four times, allowing us to measure the atomic state for varying atom numbers. Finally, the atoms are removed from the trap using resonant light, and calibration measurements are performed [see Fig. 2b]. To obtain the required statistics the experiment is repeated more than a hundred thousand times. The atomic tomography method described above is an atomic analog of homodyne detection of optical fields [24]: the strong local oscillator field is represented by the large number of atoms in the $|\uparrow\rangle$ state, and the quantum field is formed by the single $|\downarrow\rangle$ state atom. The 50:50 beam splitter is realized by the $\pi/2$ microwave pulse, and the intensity-difference measurement is implemented by the measurement of ΔN .

In order to enhance the probability of forward scattering a photon in the desired channel $|\uparrow\rangle \rightarrow F' = 4 \rightarrow |\downarrow\rangle$ a bias magnetic field of $B = 20.5$ G in the z direction [see Fig. 2a] is applied [22]. Polarization and frequency filtering in the heralding photon path (see Fig. 2a) is used to discriminate the unwanted decay channels originating from $F' = 4$. A polarizing beam splitter cube (PBS), attenuating π -polarized light by $1/(7 \times 10^3)$, suppresses anti-Stokes photons leading to $|F = 3, 4, m_F = \pm 1\rangle$. Two consecutive Fabry-Pérot cavities with a finesse of $\mathcal{F} = 300$ and a linewidth of $\delta\nu_c = 26$ MHz filter out photons corresponding to decays into $F = 4$ states with a contrast of $1/(2.7 \times 10^8)$. The decays into $|F = 3, m_F = \pm 2\rangle$ cannot be filtered out and present a limitation on the purity of the state [22].

IV. ANALYSIS

The variable $\hat{J}_z \propto \Delta N$ is determined from the differential phase shift $\tilde{\phi}_i$ imprinted by the atoms onto two collinear laser beams of different frequency in a MZI [12]. The first step of the state analysis is to calibrate the optical phase fluctuations to the atomic projection noise. Each measurement of $\tilde{\phi}_i$ is referenced to an optimally weighted average of 12 measurements on an ensemble in $|\Psi'_0\rangle$ in order to reduce the effect of slow drifts in probe powers. A small additional amount (9%) of light shot noise and atomic projection noise from these reference measurements causes a slight decrease of the detection efficiency [see Fig. 3 and Appendix A: Technical fluctuations].

A noise scaling analysis [8] confirms a predominant linear scaling of the atomic noise with N_a , which is characteristic for the atomic projection noise [see Fig. 3]. This

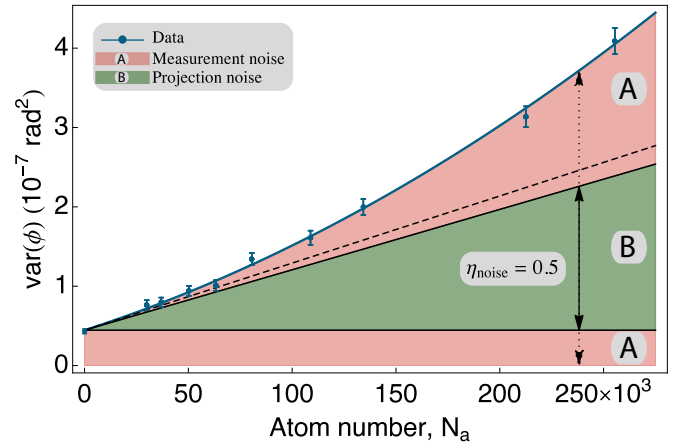


FIG. 3. (Color online) Variance of the measured optical phase shift ϕ as a function of the atom number. Different noise contributions are distinguished by a scaling analysis. The dominating linear part (dashed line) corresponds to atomic quantum projection noise; the quadratic and constant contributions (A) originate from technical fluctuations and light shot noise. Nine percent of the projection noise originates from noise-canceling reference measurements; the remaining fraction (B) constitutes $\eta_{\text{noise}} = 50\%$ of the total noise.

linear scaling with N_a is analogous to linear noise scaling with the local oscillator power in photonic homodyne measurements. For larger N_a , we observe classical noise with its quadratic scaling. The main contribution to this noise comes from frequency fluctuations of the excitation pulse which cause classical fluctuations in the atom number difference between the $F = 3$ and $F = 4$ hyperfine manifolds. Additionally, in the bias magnetic field the $|\uparrow\rangle \leftrightarrow |\downarrow\rangle$ transition frequency becomes sensitive to magnetic fields (17.5 kHz/G), such that magnetic-field fluctuations can affect the quality of the microwave pulses.

The second part of our analysis addresses the comparison of the \hat{J}_z probability distributions of states $|\Psi'_0\rangle$ and $|\Psi'_1\rangle$. Here we include only the data with $N_a > 2 \times 10^5$, where the probability of detecting the heralding photon is the highest. In order to compensate for slow drifts of the light-atom coupling strength, we introduce a noise normalization procedure and divide each ΔN measurement by the standard deviation of the neighboring $M = 200$ measurement outcomes. This allows us to locally normalize the variance to unity for events where *no* heralding photon was detected. The results for the normalized variances Z for the two states as a function of the number of samples are presented in Fig. 4. We find

$$\text{var}(Z^{\text{no click}}) = 1.02 \pm 0.02 \quad (4)$$

$$\text{var}(Z^{\text{click}}) = 1.24 \pm 0.08, \quad (5)$$

where the errors correspond to one standard deviation of the variance estimator (see Appendix B: State discrimination). As expected from our normalization procedure, in the case of no heralding photon, we obtain the unity variance. In the case of the presence of the heralding

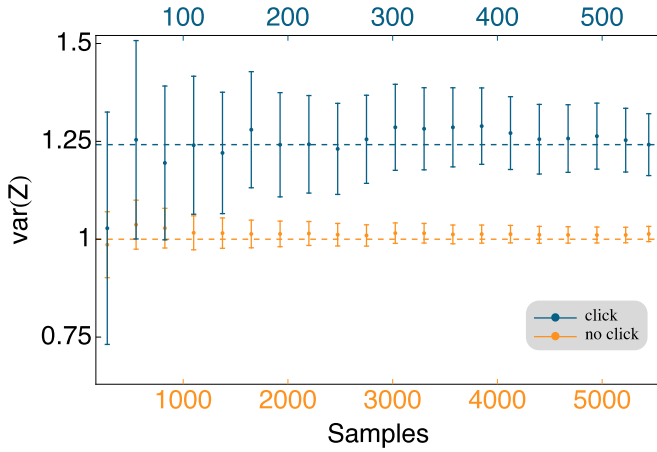


FIG. 4. (Color online) Cumulative statistics for the variance of the measurement outcomes of ΔN for the two created states, showing an increased variance for heralding events. The sample variance is plotted against the number of observations with a heralding photon (no heralding photon) as depicted on the top (bottom) axis.

photon, a statistically significant increase of 24 % in the variance is observed.

Heralding errors convert the pure target state into a statistical mixture described by a density operator

$$\hat{\rho} = p |\Psi'_1\rangle \langle \Psi'_1| + (1 - p) |\Psi'_0\rangle \langle \Psi'_0|. \quad (6)$$

Here p is the classical probability that $|\Psi'_1\rangle$ is actually prepared when a photon is detected. For state $\hat{\rho}$ we would expect

$$\begin{aligned} \text{var}(\Delta N)_{\hat{\rho}} &= p \langle \Psi'_1 | 4\hat{J}_z^2 | \Psi'_1 \rangle + (1 - p) \langle \Psi'_0 | 4\hat{J}_z^2 | \Psi'_0 \rangle \\ &= 3pN_a + (1 - p)N_a. \end{aligned} \quad (7)$$

Heralding errors which reduce the purity of the state include the detector dark counts with $p_{\text{dark}} = 0.13p_{\text{click}}$, leakage of the excitation pulse through the filters with $p_{\text{ext}} = 0.38p_{\text{click}}$, and unfiltered photons originating from the decay into $|F = 3, m_F = \pm 2\rangle$ states with $p_{\text{decay}} = 0.11p_{\text{click}}$. Here $p_{\text{click}} = 6.7 \times 10^{-3}$ is the observed photon counting probability per excitation pulse. For the purity of the created state we find

$$p_{\text{state}} = 1 - \frac{p_{\text{dark}} + p_{\text{decay}} + p_{\text{ext}}}{p_{\text{click}}} = 38\%. \quad (8)$$

With a stronger suppression of the false-positive events by better filtering cavities a state purity exceeding 70 % can be foreseen.

The quantum efficiency of the atomic state detection is finite due to several effects which add state-independent Gaussian noise. It is well known [28] that when homodyne quadrature measurements are normalized to a vacuum state with added uncorrelated Gaussian noise, this effectively decreases the quantum efficiency η_Q of the detection. This decrease can be modeled by assuming a vacuum admixture of $1 - \eta_Q$ followed by an ideal detection. In

our experiment such additional noise that is uncorrelated with the quantum state of interest [red areas (dark gray) in Fig. 3] originates from the electronic detector noise, photon shot noise [22, 29], classical fluctuations in the atomic state initialization, and the noise from the 12 reference measurements (Appendix A: Technical fluctuations). These noise sources lead to an effective detection quantum efficiency of $\eta_{\text{noise}} = 50\%$ as indicated in Fig. 3. The non-perfect overlap between the excitation and the photon-collection modes contributes $\eta_{\text{mm}} = 75\%$. Spontaneous emission of photons into modes which do not interfere with the single excitation acts similar to the imperfect spatial overlap with the local oscillator in photonic homodyning and leads to the factor $\eta_{\text{scatter}} = 77\%$. Finally, the phase mismatch between the prepared spin wave and the detection mode caused by the inhomogeneous ac-Stark shift induced by the excitation beam and the refractive index of the atomic ensemble leads to a minor correction of $\eta_{\text{inhom}} = 92\%$ (see Appendix D: Phase mismatch). The total efficiency of the state detection is given by $\eta_Q = \eta_{\text{noise}}\eta_{\text{mm}}\eta_{\text{inhom}}\eta_{\text{scatter}} = 27\%$. The expected variance of the created state can then be found as $\text{var}(\Delta N)_{\hat{\rho}}/N_a = 3p_{\text{expect}} + (1 - p_{\text{expect}}) = 1.20$, where $p_{\text{expect}} = p_{\text{state}}\eta_Q$, in good agreement with the experimental value.

The contribution of multiple excitations of the spin-wave mode which, in principle, can strongly affect the results [30, 31] is negligible in our experiment. This is a result of a relatively high probability to detect photons scattered into the detection mode of $p_d = 18\%$ combined with a photon-number-resolving detector (the detector dead time of 50 ns is short compared to the 2.5 μs excitation pulse duration). A detailed calculation (Appendix E: Multiple spin-wave excitations) reveals that, on the condition of a heralding photon, the probability to find more than one atomic excitation is $p(n > 1|\text{click}) = 9 \times 10^{-3}$ which increases $\text{var}(Z^{\text{click}})$ by 2 %. The two-excitation contribution amounts to less than 17 % of that of a coherent spin state with the same mean excitation number.

V. CONCLUSION

In conclusion, we have implemented a hybrid discrete-continuous protocol where a collective single spin excitation heralded by the detection of a single photon is characterized by a direct measurement of a collective continuous-variable atomic operator. Although, in general, an observed increase in the variance of the atomic operator could be due to classical reasons, such as an admixture of a thermal state, in our experiment the increase is solely due to the detection of a scattered single photon. Even stronger evidence of the successful generation of a single excitation state requires determination of higher-order statistical moments, which in turn demands a higher purity of the produced quantum state [24, 32, 33]. Steps towards this goal could include a stronger light-atom coupling achievable in ensembles

trapped around nanofibers [34, 35], atoms coupled to optical resonators [9, 36, 37], or photonic structures [38, 39]. Furthermore, a better suppression of false photon counts and using atoms with a simpler level structure (e.g. ^{87}Rb) could help. These improvements of the method should allow for observation of a negative Wigner function of a macroscopic atomic ensemble, certifying its non-classical properties [26]. Such a state is a building block for atomic Schrödinger's cat states [20]; it can be used in precision measurements [21, 40] and provides a non-Gaussian resource for future quantum information processing [25].

ACKNOWLEDGMENTS

This work is funded by the Danish National Research Foundation, EU projects SIQS, MALICIA, ERC grant INTERFACE, and DARPA through the project QuASAR. We thank Emil Zeuthen and Anders S. Sørensen for helpful discussions.

Appendix A: Technical fluctuations

Using the dual-color QND measurement we prepare and probe our ensemble, obtaining measurement outcomes $\tilde{\phi}_i$. To eliminate technical fluctuations, we subtract the baseline of the empty interferometer. Further noise reduction is achieved by performing 12 reference measurements $\{\varphi_i^j\}_{j \in \{-6, \dots, -1, 1, \dots, 6\}}$ on a $|\Psi_0'\rangle$ state, six each immediately before and after ϕ_i is measured. Since these measurements are performed on independently prepared atomic ensembles, all correlations between them are of technical nature. We therefore decorrelate $\tilde{\phi}_i$ from its reference measurements φ_i^j by subtracting the correlated noise contributions:

$$\phi_i = \tilde{\phi}_i - \sum_{\substack{j=-6 \\ j \neq 0}}^6 w_j \varphi_i^j. \quad (\text{A1})$$

The 12 weight factors w_j are chosen such that the sample variance $\text{var}(\{\phi_i\})$ is minimized. Since each reference measurement contains both the full (uncorrelated) atomic projection and shot noise, this procedure not only reduces technical fluctuations but also adds $\sum_j w_j^2 = 0.09$ units of projection and shot noise to each ϕ_i measurement. This decreases the state detection efficiency η_{noise} , as explained in Sec. IV. Analysis. The above choice of w_j guarantees an optimization of this trade-off.

Appendix B: State discrimination

To compare the measurement statistics for the two created states $|\Psi_1'\rangle$ and $|\Psi_0'\rangle$, we only consider data with $N_a > 2 \times 10^5$. For these high-atom-number realizations we obtain a high η_{noise} , which directly leads to a large

increase in the difference of variances, as explained in Sec. IV. Analysis.

As our data are acquired over a duration of 2 weeks, we observe slow, long-term changes in the variance of the measurements. These are caused mainly by drifts in the relative optical power of the MOT beams, changes in the background vapor pressure due to operation of the cesium dispensers, and accumulation of dust particles in the shared optical path of the strong, focused dipole trap, excitation, and probe beams. We therefore perform a local noise normalization to avoid long-term drifts in the variance of our measurements.

For each correlation-removed measurement outcome ϕ_i we compute the sample variance of the M surrounding experiments:

$$Y_i \equiv \text{var}(\{\phi_{i-M/2}, \dots, \phi_{i+M/2}\}), \quad (\text{B1})$$

and we use this to normalize the variance of ϕ_i to the surrounding data points:

$$Z_i \equiv \frac{\phi_i}{\sqrt{Y_i}}. \quad (\text{B2})$$

The Z_i originating from a $|\Psi_0'\rangle$ measurement, by this construction, have an average variance of ≈ 1 since $p_{\text{click}} \ll 1$; that is Y_i contain almost entirely no-click events.

Our final parameter of interest is the sample variance of a set of Z_i

$$W_{\mathbf{L}} \equiv \text{var}(\{Z_i\}_{i \in \mathbf{L}}), \quad (\text{B3})$$

both for the sets of indices $\mathbf{L}^{\text{click}} = \{i : \text{click detected}\}$ and $\mathbf{L}^{\text{no click}} = \{i : \text{no click}\}$. In the following we focus on estimating the statistical uncertainty $\delta W_{\mathbf{L}}$ on $W_{\mathbf{L}}$ and denote with $L = |\mathbf{L}|$ the number of samples used in the calculation.

Due to the finite number of points used in estimating Y_i there is a statistical uncertainty on this estimator which carries over to Z_i . Since all ϕ_i from within the range $[i - M/2, \dots, i + M/2]$ can be considered independently and identically distributed, we can give the uncertainty of Y_i simply by the mean-square error (MSE) of the variance estimator and find

$$\delta Y_i = \sqrt{\frac{2}{M-1}} Y_i. \quad (\text{B4})$$

This allows us to find the variance of each of the Z_i by Taylor expansion around $\langle Y_i \rangle$ as

$$\text{var}(Z_i) = \left(1 + \frac{1}{4} \frac{2}{M+1}\right) \text{var}\left(\frac{\phi_i}{\langle Y_i \rangle}\right). \quad (\text{B5})$$

One complication is that within a range of M neighboring experiments the Z_i are not statistically independent any longer due to our normalization procedure. As can be seen from (B5), by ensuring that $M \gg 1$, we can make the contribution of correlated noise to each Z_i negligibly small. If, additionally, we either choose $L \gg M$ or ensure

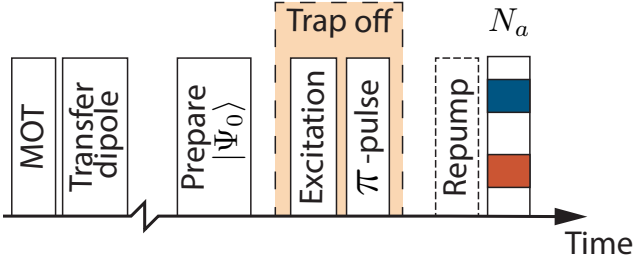


FIG. 5. (Color online) Experimental sequence in order to estimate η_{scatter} .

that the members of \mathbf{L} are spaced much farther than M on average, $W_{\mathbf{L}}$ is an unbiased estimator of the Z_i variance, and its uncertainty is

$$\delta W_{\mathbf{L}} = \sqrt{\frac{2}{L-1}} W_{\mathbf{L}}, \quad (\text{B6})$$

which is simply the MSE on the variance estimator for L independent samples.

We confirm all our error estimates experimentally both by dividing our data set into subsets and evaluating the standard deviation of the variance estimates and by the bootstrapping method (resampling).

Appendix C: Scattering

To determine η_{scatter} , the fraction of atoms that scatter a photon from the excitation pulse, we perform a separate calibration experiment [see Fig. 5]. First we prepare all atoms in the $|\uparrow\rangle$ state (see Sec. III. Experiment). While the trap is switched off we send the excitation pulse followed by a microwave π pulse and an optional repumping pulse, resonant to the $F = 3 \rightarrow F' = 4$ transition. Finally the number of atoms N_a in $F = 4$ is determined. In the presence of the repumping pulse, all atoms in the trap are detected, whereas in the absence of the repumping pulse only atoms scattered into the $|F = 4, m_F \neq 0\rangle$ and $|F = 3, m_F = 0\rangle$ states are measured. Finally, using the relevant Clebsch-Gordan coefficients to determine the fraction of atoms scattering into each Zeeman state, we can find the fraction of atoms that undergo a scattering event to be $1 - \eta_{\text{scatter}} = 23\%$.

Appendix D: Phase mismatch

Inhomogeneous phase shifts can reduce the interference visibility $\eta_{\text{inhom}} = \eta_{\text{phase}} \eta_{\text{ac-Stark}}$. Here we consider two effects.

1. Longitudinal phase profile

The first effect concerns the refractive index mismatch between the scattered single photon and the excitation beam. In our one-dimensional model we describe this by a position dependent phase difference $\theta(y) = \Delta k y$, where $\Delta k = k_{\mu\text{-wave}} + k_{\text{exct}} - k_{\text{photon}}$ is the wave-vector mismatch between microwave-, excitation- and heralding-photon fields. Since no atoms reside in $|\downarrow\rangle$, the atomic phase mismatch emerges exclusively from the optical phase shift of the excitation beam $\chi_{\text{exct}} = \theta(L_a)$.

For the sake of simplicity we assume a homogeneous atomic density distribution and average the phase over the length of the atomic ensemble L_a :

$$\eta_{\text{phase}} = \left| \frac{1}{L_a} \int_0^{L_a} e^{-i\theta(y)} dy \right|^2 = \text{sinc}^2(\chi_{\text{exct}}/2) \quad (\text{D1})$$

We can relate the excitation beam phase shift χ_{exct} to the measured phase shift χ_{probe} of the QND probe during the atom number measurement. Let α_0 denote the resonant optical depth on a closed transition. Then, light traveling through a medium with optical depth α_0 , detuned by a frequency Δ_i with respect to a transition with relative strength \wp_i will experience an optical phase shift,

$$\chi(\Delta, \alpha_0) = \frac{\alpha_0}{4} \sum_i \wp_i \frac{\Delta_i}{\Delta_i^2 + (\Gamma/2)^2}. \quad (\text{D2})$$

When all our atoms are pumped into $F' = 4$, with the probe beam we measure an optical phase shift corresponding to $\alpha_0 = 31$, from which, using the Clebsch-Gordan coefficients and the detuning corresponding to our excitation beam, we obtain $\chi_{\text{exct}} = 42^\circ$, which gives $\eta_{\text{phase}} = 95\%$.

2. Transversal phase profile

The off-resonant excitation pulse leads to an ac-Stark shift, both of the $|\uparrow\rangle$ state and the excited states. Only the spatially inhomogeneous shift of the $|\uparrow\rangle$ state affects the spin wave coherence, which reduces the interference visibility. Since the longitudinal extent of our atomic ensemble is short compared to the Rayleigh length of the light beams, we restrict our model to transversal effects, which can be evaluated as [1]

$$\eta_{\text{ac-Stark}} = \frac{\int \left| \iint \varrho(x, z) I(x, z)^2 e^{-i\omega_{\text{LS}}(x, z)t} dx dz \right|^2 dt}{\tau \left| \iint \varrho(x, z) I(x, z)^2 dx dz \right|^2} \quad (\text{D3})$$

where $I(x, z)$ denotes the transverse Gaussian intensity profile of the excitation beam, $\varrho(x, z)$ is the atomic column density, $\omega_{\text{LS}}(x, y) \propto I(x, z)$ is the ac-Stark shift of the $|\uparrow\rangle$ state, and τ is the excitation pulse duration. Numerically evaluating the above allows us to estimate the effect and we find $\eta_{\text{ac-Stark}} = 97\%$.

Appendix E: Multiple spin-wave excitations

When the single photon counter reports a “click”, this can originate from dark counts, leakage of excitation photons, or actual Stokes photons scattered from the atomic ensemble (either from the desired or from other unwanted transitions). To investigate the influence of multiple-Stokes-photon events on our analysis, we calculate $p(n|1\text{click})$. This is the probability that the atomic ensemble scattered n Stokes photons with an energy corresponding to a decay to the state $|\downarrow\rangle$ exactly into the detection spatial mode, on the condition of detecting a single click. Since the detector dead time of 50 ns is much smaller than the 2.5 μs excitation pulse length, we effectively have a number-resolving photon detection. By Bayes’ rule we have

$$p(n|1\text{click}) = \frac{p(n)p(1\text{click}|n)}{p(1\text{click})}, \quad (\text{E1})$$

where $p(n)$ is the probability to scatter n photons with an energy corresponding to a decay to the state $|\downarrow\rangle$ exactly into the detection spatial mode and $p(1\text{click})$ is the probability to detect exactly one click. For a two-mode squeezed vacuum state the photon number statistics in the individual modes is thermal [41]. Thus the probability to find n Stokes photons corresponding to a decay into $|\downarrow\rangle$ is given by

$$p_{S0}(n) = (1 - p_0) p_0^n, \quad (\text{E2})$$

where p_0 is the probability to generate at least one of the desired Stokes photons.

Dark counts and leakage photons from the excitation pulse follow a Poisson distribution

$$p_{\text{DE}}(n) = \frac{p_{\text{f}}^n e^{-p_{\text{f}}}}{n!}, \quad (\text{E3})$$

where p_{f} is the mean number of such false-positive clicks in the absence of atoms. Stokes photons corresponding to decay into $|F = 3, m_F = \pm 2\rangle$ are not filtered out and therefore also cause false positives. Their generation is distributed as

$$p_{S2}(n) = (1 - p_2) p_2^n, \quad (\text{E4})$$

where p_2 is the probability to scatter at least one photon corresponding to a decay to $|F = 3, m_F = \pm 2\rangle$.

Finally, we introduce $p_{\text{d}} = 0.8^2 \times 0.56 \times 0.5$, the probability that a single Stokes photon in the detection mode

causes an (additional) click which is given by the product of the transmission coefficients through the filter cavities, through other optics, and by the detector quantum efficiency. The complementary probability is denoted $\tilde{p}_{\text{d}} = 1 - p_{\text{d}}$.

Then the probability for detecting n additional clicks due to unwanted $|F = 3, m_F = \pm 2\rangle$ Stokes photons is

$$p_{\text{DS2}}(n) = \sum_{k=n}^{\infty} p_{S2}(k) \binom{k}{k-n} \tilde{p}_{\text{d}}^{k-n} p_{\text{d}}^n \quad (\text{E5})$$

$$= \frac{(1 - p_2) (p_2 p_{\text{d}})^n}{(1 - p_2 \tilde{p}_{\text{d}})^{n+1}}. \quad (\text{E6})$$

The probability to find no false-positive events is $p_{\text{F}}(0) = p_{\text{DE}}(0) p_{\text{DS2}}(0)$, whereas the probability to find exactly one false positive is $p_{\text{F}}(1) = p_{\text{DE}}(1) p_{\text{DS2}}(0) + p_{\text{DE}}(0) p_{\text{DS2}}(1)$.

With this, $p(1\text{click}|n)$, the probability to detect exactly one click when the atoms scatter n photons corresponding to the desired $|\downarrow\rangle$ decay, is made up of two cases: (a) exactly one of the n photons makes it through the filtering optical elements and causes a click in the detector while simultaneously no false-positive counts are detected, and (b) none of the n photons cause a detector click while exactly one false positive count is detected:

$$p(1\text{click}|n) = n p_{\text{d}} \tilde{p}_{\text{d}}^{n-1} p_{\text{F}}(0) + \tilde{p}_{\text{d}}^n p_{\text{F}}(1). \quad (\text{E7})$$

Using the relation $\sum_{n=0}^{\infty} p(n|1\text{click}) = 1$, from (E1) we can determine $p(1\text{click})$ and obtain:

$$p(n|1\text{click}) = \frac{\tilde{p}_{\text{d}}^n p_0^n (1 - \tilde{p}_{\text{d}} p_0) \left(n \frac{p_{\text{d}}}{\tilde{p}_{\text{d}}} + p_{\text{f}} + \frac{p_{\text{d}} p_2}{1 - \tilde{p}_{\text{d}} p_2} \right)}{p_{\text{f}} + \frac{p_{\text{d}} p_2}{1 - \tilde{p}_{\text{d}} p_2} + \frac{p_{\text{d}} p_0}{1 - \tilde{p}_{\text{d}} p_0}}. \quad (\text{E8})$$

Since we know $p_{\text{f}} = p_{\text{dark}} + p_{\text{exct}}$ from reference measurements without atoms and $p_2 = 0.3 p_0$ from the ratio of the transition strengths, we can deduce $p_0 = p_{\text{forward}} = 0.014$ and obtain the probability $p(n|1\text{click})$ for different n :

$$p(n = 0|1\text{click}) = 0.606 \quad (\text{E9})$$

$$p(n = 1|1\text{click}) = 0.385 \quad (\text{E10})$$

$$p(n = 2|1\text{click}) = 0.009 \quad (\text{E11})$$

Since all multi-excitation contributions together only amount to 2.4 % of the single excitation contribution, we can safely neglect their influence in our analysis.

-
- [1] K. Hammerer, A. Sørensen, and E. Polzik, *Rev. Mod. Phys.* **82**, 1041 (2010).
 - [2] H. J. Kimble, *Nature* **453**, 1023 (2008).
 - [3] K. S. Choi, A. Goban, S. B. Papp, S. J. van Enk, and H. J. Kimble, *Nature* **468**, 412 (2010).

- [4] A. MacRae, T. Brannan, R. Achal, and A. I. Lvovsky, *Phys. Rev. Lett.* **109**, 033601 (2012).
- [5] L. M. Duan, M. D. Lukin, J. I. Cirac, and P. Zoller, *Nature* **414**, 413 (2001).
- [6] H. P. Specht, C. Nölleke, A. Reiserer, M. Uphoff,

- E. Figueroa, S. Ritter, and G. Rempe, *Nature* **473**, 190 (2011).
- [7] H. Krauter, D. Salart, C. A. Muschik, J. M. Petersen, H. Shen, T. Fernholz, and E. S. Polzik, *Nature Physics* **9**, 400 (2013).
- [8] J. Appel, P. J. Windpassinger, D. Oblak, U. Busk Hoff, N. Kjærgaard, and E. S. Polzik, *P. Natl. Acad. Sci.* **106**, 10960 (2009).
- [9] I. D. Leroux, M. H. Schleier-Smith, and V. Vuletić, *Phys. Rev. Lett.* **104**, 073602 (2010).
- [10] T. Fernholz, H. Krauter, K. Jensen, J. F. Sherson, A. S. Sørensen, and E. S. Polzik, *Phys. Rev. Lett.* **101**, 073601 (2008).
- [11] W. Wasilewski, K. Jensen, H. Krauter, J. J. Renema, M. V. Balabas, and E. S. Polzik, *Phys. Rev. Lett.* **104**, 133601 (2010).
- [12] A. Louchet-Chauvet, J. Appel, J. J. Renema, D. Oblak, N. Kjærgaard, and E. S. Polzik, *New. J. Phys.* **12**, 065032 (2010).
- [13] M. Koschorreck, M. Napolitano, B. Dubost, and M. W. Mitchell, *Phys. Rev. Lett.* **104**, 093602 (2010).
- [14] C. Simon, M. Afzelius, J. Appel, A. Boyer de La Giroday, S. J. Dewhurst, N. Gisin, C. Y. Hu, F. Jelezko, S. Kröll, J. H. Müller, J. Nunn, E. S. Polzik, J. G. Rarity, H. de Riedmatten, W. Rosenfeld, A. J. Shields, N. Sköld, R. M. Stevenson, R. Thew, I. A. Walmsley, M. C. Weber, H. Weinfurter, J. Wrachtrup, and R. J. Young, *Eur. Phys. J. D* **58**, 1 (2010).
- [15] J. S. Neergaard-Nielsen, B. M. Nielsen, C. Hettich, K. Mølmer, and E. S. Polzik, *Phys. Rev. Lett.* **97**, 083604 (2006).
- [16] A. Ourjoumtsev, H. Jeong, R. Tualle-Brouiri, and P. Grangier, *Nature* **448**, 784 (2007).
- [17] S. Takeda, T. Mizuta, M. Fuwa, P. van Loock, and A. Furusawa, *Nature* **500**, 315 (2013).
- [18] A. I. Lvovsky, R. Ghobadi, A. Chandra, A. S. Prasad, and C. Simon, *Nature Physics* **9**, 541 (2013).
- [19] N. Bruno, A. Martin, P. Sekatski, N. Sangouard, R. T. Thew, and N. Gisin, *Nature Physics* **9**, 545 (2013).
- [20] J. B. Brask, I. Rigas, E. S. Polzik, U. L. Andersen, and A. S. Sørensen, *Phys. Rev. Lett.* **105**, 160501 (2010).
- [21] R. McConnell, H. Zhang, S. Čuk, J. Hu, M. H. Schleier-Smith, and V. Vuletić, *Physical Review A* **88**, 063802 (2013).
- [22] S. L. Christensen, J. B. Béguin, H. L. Sørensen, E. Bookjans, D. Oblak, J. H. Müller, J. Appel, and E. S. Polzik, *New J. Phys., Focus issue on Quantum Tomography* **15**, 015002 (2013).
- [23] T. Holstein and H. Primakoff, *Phys. Rev.* **58**, 1098 (1940).
- [24] A. I. Lvovsky and M. G. Raymer, *Rev. Mod. Phys.* **81**, 299 (2009).
- [25] M. Ohliger and J. Eisert, *Phys. Rev. A* **85**, 062318 (2012).
- [26] E. Kot, N. Grønbech-Jensen, B. M. Nielsen, J. S. Neergaard-Nielsen, E. S. Polzik, and A. S. Sørensen, *Phys. Rev. Lett.* **108**, 233601 (2012).
- [27] J. P. Dowling, G. S. Agarwal, and W. P. Schleich, *Phys. Rev. A* **49**, 4101 (1994).
- [28] J. Appel, D. Hoffman, E. Figueroa, and A. I. Lvovsky, *Phys. Rev. A* **75**, 035802 (2007).
- [29] T. Kiesel, W. Vogel, S. L. Christensen, J.-B. Béguin, J. Appel, and E. S. Polzik, *Phys. Rev. A* **86**, 042108 (2012).
- [30] J. Laurat, H. de Riedmatten, D. Felinto, C.-W. Chou, E. W. Schomburg, and H. J. Kimble, *Opt. Express* **14**, 6912 (2006).
- [31] A. Kuzmich, W. P. Bowen, A. D. Boozer, A. Boca, C. W. Chou, L.-M. Duan, and H. J. Kimble, *Nature* **423**, 731 (2003).
- [32] B. Dubost, M. Koschorreck, M. Napolitano, N. Behbood, R. J. Sewell, and M. W. Mitchell, *Phys. Rev. Lett.* **108**, 183602 (2012).
- [33] R. Schmied and P. Treutlein, *New. J. Phys.* **13**, 065019 (2011).
- [34] E. Vetsch, D. Reitz, G. Sagué, R. Schmidt, S. T. Dawkins, and A. Rauschenbeutel, *Phys. Rev. Lett.* **104**, 203603 (2010).
- [35] C. Lacroûte, K. S. Choi, A. Goban, D. J. Alton, D. Ding, N. P. Stern, and H. J. Kimble, *New. J. Phys.* **14**, 023056 (2012).
- [36] H. Zhang, R. McConnell, S. Čuk, Q. Lin, M. H. Schleier-Smith, I. D. Leroux, and V. Vuletić, *Phys. Rev. Lett.* **109**, 133603 (2012).
- [37] Y. Colombe, T. Steinmetz, G. Dubois, F. Linke, D. Hunger, and J. Reichel, *Nature* **450**, 272 (2007).
- [38] J. D. Thompson, T. G. Tiecke, N. P. de Leon, J. Feist, A. V. Akimov, M. Gullans, A. S. Zibrov, V. Vuletić, and M. D. Lukin, *Science* **340**, 1202 (2013).
- [39] A. Goban, C.-L. Hung, S.-P. Yu, J. D. Hood, J. A. Muniz, J. H. Lee, M. J. Martin, A. C. McClung, K. S. Choi, D. E. Chang, O. Painter, and H. J. Kimble, ArXiv e-prints (2013), [arXiv:1312.3446](https://arxiv.org/abs/1312.3446).
- [40] C. Simon and E. S. Polzik, *Phys. Rev. A* **83**, 040101 (2011).
- [41] C. T. Lee, *Phys. Rev. A* **42**, 1608 (1990).